

Deformable 3D Gaussians for High-Fidelity Monocular Dynamic Scene Reconstruction

Ziyi Yang^{1,2} Xinyu Gao¹ Wen Zhou² Shaohui Jiao² Yuqing Zhang¹ Xiaogang Jin^{1†}

¹State Key Laboratory of CAD&CG, Zhejiang University ²ByteDance Inc.

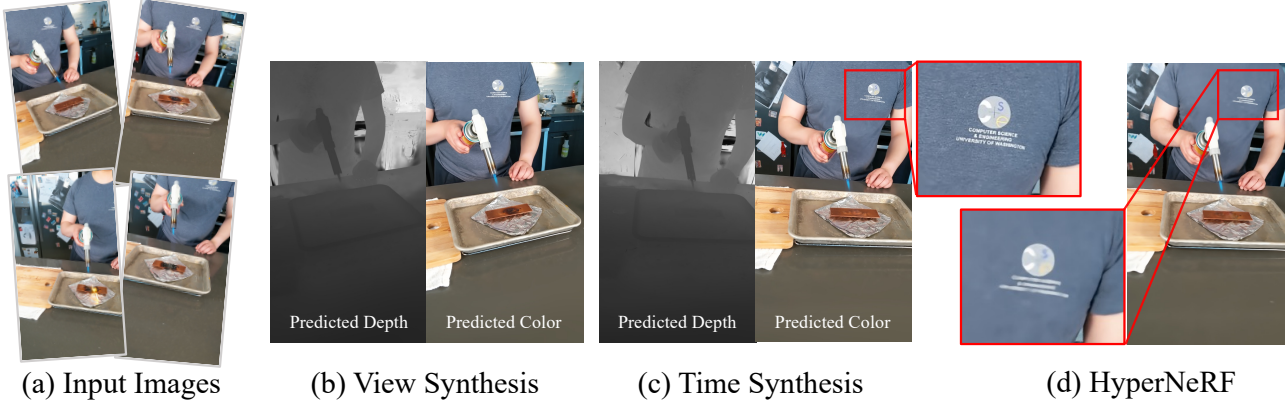


Figure 1. Given a set of monocular multi-view images and camera poses (a), our proposed method can reconstruct accurate scene geometry and render high-quality images in both the view synthetic (b) and time synthetic (c) tasks. In real-world datasets with intricate details, our method outperforms *HyperNeRF* [30] (d) in terms of rendering quality and time performance.

Abstract

Implicit neural representation has opened up new avenues for dynamic scene reconstruction and rendering. Nonetheless, state-of-the-art methods of dynamic neural rendering rely heavily on these implicit representations, which frequently struggle with accurately capturing the intricate details of objects in the scene. Furthermore, implicit methods struggle to achieve real-time rendering in general dynamic scenes, limiting their use in a wide range of tasks. To address the issues, we propose a deformable 3D Gaussians Splatting method that reconstructs scenes using explicit 3D Gaussians and learns Gaussians in canonical space with a deformation field to model monocular dynamic scenes. We also introduced a smoothing training mechanism with no extra overhead to mitigate the impact of inaccurate poses in real datasets on the smoothness of time interpolation tasks. Through differential gaussian rasterization, the deformable 3D Gaussians not only achieve higher rendering quality but also real-time rendering speed. Experiments show that our method outperforms existing meth-

ods significantly in terms of both rendering quality and speed, making it well-suited for tasks such as novel-view synthesis, time synthesis, and real-time rendering. We plan to release our code and data soon.

1. Introduction

High-quality reconstruction and photorealistic rendering of *dynamic scenes* from a set of input images is critical for a variety of applications, including augmented reality/virtual reality (AR/VR), 3D content production, and entertainment. For modeling dynamic scenes, existing methods [9, 14, 17, 39] frequently use mesh-based representations. Nonetheless, they run into a number of issues, including a lack of detail and realism, a lack of semantic information, and difficulties dealing with topological changes. Implicit scene representations, exemplified by NeRF [27], have demonstrated impressive performance in areas such as novel viewpoint synthesis, scene reconstruction, and light decomposition with the rise of neural rendering methods.

To improve inference efficiency in NeRF-based static

scenes, researchers have developed a variety of acceleration methods, including grid-based structures [4, 7, 45] and pre-computation strategies [43, 50]. Notably, by incorporating hash encoding, Instant-NGP [28] has achieved rapid training. In terms of quality improvement, mipNeRF [2] pioneered an effective anti-aliasing method, which was later incorporated into the grid-based approach by zipNeRF [4]. 3D-GS [15] recently extended the volumetric rendering equation proposed in NeRF [27] to accommodate point clouds. This has enabled real-time rendering that matches or even exceeds the rendering quality of Mip-NeRF [2], elevating the neural scene representation paradigm. However, this method has difficulties modeling *dynamic scenes*, and its CUDA-specific rasterization pipeline adds to the complexities of adapting to such dynamic scenes.

The implicit representation has also been used in the representation of dynamic scenes. To handle the motion part in a dynamic scene, entangled methods [42, 48] conditioned NeRF on a time variable. Disentangled methods [22, 29, 30, 33, 38] use a deformation field to fit a function mapping the point coordinates at a specific time to canonical space to model a scene in canonical space. This decoupled modeling approach can effectively represent scenes with non-dramatic action variations, and it will be used as a primary strategy in future works in modeling dynamic scenes. Regardless of method category, a naive implicit representation for dynamic scene representation is inefficient and ineffective, characterized not only by slow convergence but also by a proclivity for overfitting. Many works in modeling dynamic scenes, inspired by the classic NeRF acceleration research, have incorporated discrete structures such as voxel-grid [11, 37] or planes [35] to alleviate the difficulties in representing the deformation field, significantly accelerating the training speed and improving modeling precision. However, methods incorporating discrete structures continue to face difficulties in achieving real-time rendering speeds and delivering high-quality outputs with adequate detail. Several factors contribute to these difficulties: To begin with, ray-casting as a rendering technique can be inefficient, especially at higher resolutions like 1080p. Second, in monocular dynamic scenarios, the camera pose for each frame can be inaccurate, particularly when determined using tools such as COLMAP [36].

In this paper, we propose a deformable 3D Gaussian framework for modeling dynamic scenes. In order to achieve generality and handle a wide range of scenes, we use a single monocular view rather than multiple view stereo (MVS) at times. Rather than reconstructing the point cloud frame by frame [25], we condition the point cloud on time and jointly train a deformation field to optimize the learnable 3D Gaussians in canonical space. Both components' gradients are derived from a customized differential gaussian rasterization pipeline. We introduced an annealed

smoothing training (AST) mechanism to reduce the impact of scene jitter caused by inaccurate poses in real datasets on the explicit point cloud representation. This not only improves the smoothness between frames in the time interpolation task, but also allows for greater detail to be rendered.

In summary, the major contributions of our work are:

- A deformable 3D Gaussian framework for modeling monocular dynamic scenes that can achieve real-time rendering while allowing for high-fidelity scene representation.
- A novel annealing smoothing training mechanism that ensures temporal smoothness while preserving dynamic details without increasing computational complexity.

2. Related Work

2.1. Neural Rendering for Dynamic Scenes

Because of its ability to produce photorealistic images, neural rendering has grown in popularity. NeRF [27], which was recently developed, enables photo-realistic novel view synthesis using MLPs. Later works use NeRF in a variety of downstream tasks, including mesh reconstruction from a collection of images [19, 44], inverse rendering [5, 24, 51], camera parameter optimization [20, 46, 47]], and few-shot learning [10, 49].

Constructing radiance fields for dynamic scenes is a critical branch in the advancement of NeRF [27], with significant implications for real-world applications. The effective encoding of temporal information is the central challenge in rendering dynamic scenes. The main issue in solving dynamic scene rendering is temporal information encoding and utilization. The encoding of temporal information is critical in determining the convergence of the radiance field, particularly in the reconstruction of monocular dynamic scenes, which inherently involves sparse reconstruction from a single viewpoint. One class of dynamic NeRF approaches models scene deformation by adding time t as an additional input to the radiance field. However, this strategy couples the positional variations induced by temporal dynamics with the radiance field, lacking the geometric prior information regarding the influence of time on the scene. Consequently, substantial regularization is required to ensure temporal consistency in the rendering results. Another category of methods [29, 30, 33] introduces a deformation field to decouple time and the radiance field, mapping point coordinates to the canonical space corresponding to time t through the deformation field. This decoupled approach facilitates the learning of substantial rigid motions and can even accommodate scenes undergoing topological structural alterations. Other methods seek

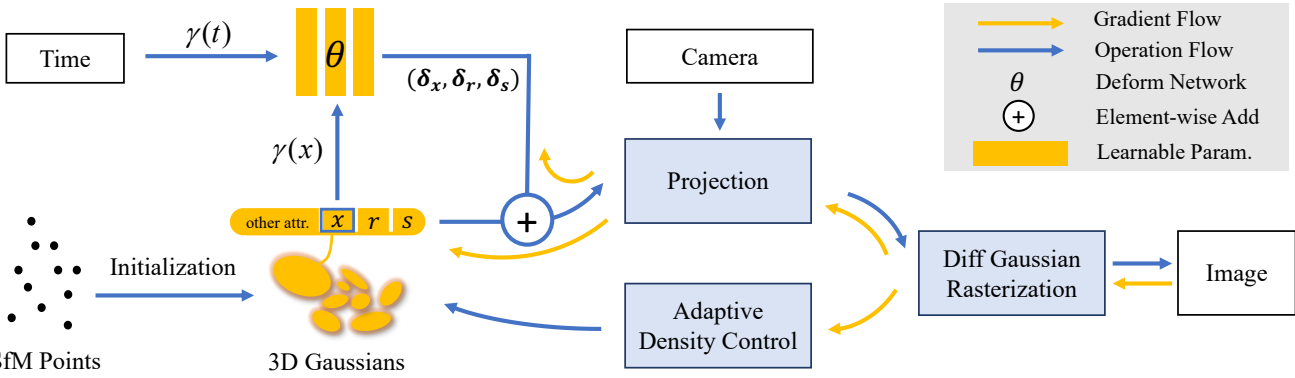


Figure 2. **Overview of our pipeline.** The optimization process begins with Structure from Motion (SfM) points derived from COLMAP or generated randomly, which serve as the initial state for the 3D Gaussians. We use the position of 3D Gaussians $\gamma(x)$ and time $\gamma(t)$ with positional encoding as input to a deformation MLP network to obtain the offset of dynamic 3D Gaussians in canonical space $(\delta_x, \delta_r, \delta_s)$. We use a warm-up phase for the 3D Gaussians during the first 3k iterations without optimizing the deformation field. Following that, we use the fast differential gaussian rasterization pipeline to perform joint optimization of the deformation field and the 3D Gaussians, as well as to adaptively control the density of the set of Gaussians.

to enhance the quality of dynamic neural rendering from various aspects, including segmenting static and dynamic objects in the scene [38, 41], incorporating depth information [1] to introduce geometric prior knowledge, introducing 2D CNN to encode scene priors [21, 32], and leveraging the redundant information in multi-view videos [18] to set up keyframe compression storage, thereby accelerating the rendering speed.

However, the current dynamic neural rendering necessitates going through an implicit Multilayer Perceptron (MLP), which is extremely unfavorable for editing the intermediate states in dynamic scenes. In this work, we will focus on the reconstruction of monocular dynamic scenes. To enhance the editability of the intermediate processes, we have decoupled the deformation field and the radiance field, while adopting differentiable rendering based on point clouds.

2.2. Acceleration of Neural Rendering

Real-time rendering has long been a pivotal objective in the field of computer graphics, a goal that is also pursued in the domain of neural rendering. A plethora of studies aiming to accelerate NeRF have explored the delicate trade-off between spatial and temporal efficiency.

Pre-computed methods [12, 34] utilize spatial acceleration structures such as spherical harmonics coefficients [50] and feature vectors [13], cached or distilled from implicit neural representation, as opposed to directly employing the neural representations themselves. A prominent technique [8] in this category transforms NeRF scenes into an amalgamation of coarse meshes and feature textures, thereby enhancing rendering velocity in contemporary mobile graphics pipelines. Nonetheless, this pre-computed approach can

incur substantial storage requisites for a single scene. Although this method can improve the inference speed, the training time is very long and the overhead is high.

Hybrid methods [4, 7, 23, 26, 40, 45] incorporate a neural component within the explicit grid. The hybrid approaches not only concurrently facilitate the acceleration of both training and inference, but also achieve results comparable to Mip-NeRF [2] and Mip-NeRF 360 [3] owing to the potent representational capacity of the grid. This grid or plane based strategy has been extended to the acceleration [11] or representation of time-conditioned 4D feature [6, 35, 37] in dynamic scene modeling and time-conditioned compact 4D dynamic scene modeling.

Recently, 3D-GS [15] has adopted a novel approach based on point cloud rendering, achieving optimal results in tasks such as new viewpoint synthesis and scene modeling, while also supporting minute-level training speeds and real-time rendering exceeding 100 FPS. However, the method employs customized differential Gaussian rasterization pipeline, which complicates its direct extension to dynamic scenes. Inspired by this, our work will unfold with a focus on the conceptual framework of point cloud rendering.

3. Method

The overview of our method is illustrated in Fig. 2. The input to our method is a set of images of a monocular dynamic scenes, together with time label and the corresponding camera poses calibrated by SfM [36] which produces a sparse point cloud as a side-effect. From these points, we create a set of 3D Gaussians $G(x, r, s, \sigma)$ defined by a position x , covariance matrix obtained from quaternion r

and scaling s , and opacity σ . The radiance field of each 3D Gaussian is represented via spherical harmonics (SH). To model the dynamic 3D Gaussians that vary over time, we decouple the 3D Gaussians and the deformation field. The deformation field takes the positions of the 3D Gaussians and the current time t as inputs, outputting δx , δr , and δs . Subsequently, we put the canonical 3D Gaussians $G(x + \delta x, r + \delta r, s + \delta s, \sigma)$ into the efficient differential gaussian rasterization, which is a tile-based rasterizer that allows α -blending of anisotropic splats. The 3D Gaussians and deformation network are optimized through the fast backward pass by tracking accumulated α values, together with the adaptive control of the Gaussian density. Experimental results show that after 30k training iterations, the position of 3D Gaussians in canonical space has stabilized. This training framework can achieve decoupling of deforming and rendering field.

3.1. Differentiable Rendering Through 3D Gaussians Splatting in Canonical Space

In order to optimize the parameters of our dynamic 3D Gaussians, we need to render the 2D images from 3D Gaussians in a differential way. In this work, we use differential gaussian rasterization pipeline proposed by [15]. The 3D Gaussians are defined by a full 3D covariance matrix Σ defined in world space centered at point center μ . Following [52], the 3D Gaussians can be projected to 2D for rendering with the following covariance matrix Σ' :

$$\Sigma' = JV\Sigma V^T J^T, \quad (1)$$

where J is the Jacobian of the affine approximation of the projective transformation and V denotes the world-to-camera (w2c) matrix.

Given that Σ only possesses practical physical significance when it is positive semi-definite. In order to reduce the learning difficulty of the 3D Gaussians, Σ is decomposed into two learnable components with quaternion r to represent rotation and 3D-vector s to represent scaling, which can be respectively transformed into the corresponding rotation matrix R and scaling matrix S . Given the rotation matrix R and scaling matrix S , the corresponding Σ is defined as:

$$\Sigma = RSS^T R^T. \quad (2)$$

After mapping the 3D Gaussians to 2D, the alpha-blend rendering based on point clouds bears a striking resemblance to the volumetric rendering equation of NeRF in terms of its formulation. The volumetric rendering equation for each pixel contributed by Gaussians is as follows:

$$C = \sum_{i \in N} T_i \alpha_i c_i, \quad (3)$$

where T_i is the transmittance defined by $\prod_{j=1}^{i-1} \alpha_j$, α_i is the alpha value for each Gaussian defined by $1 - e^{-\sigma_i \delta_i}$, and c_i

is the color of the Gaussian along the ray with the interval δ_i .

During optimization, adaptive density control is a crucial factor enabling 3D Gaussians to achieve satisfactory rendering results. On one hand, it necessitates the removal of transparent Gaussians according to the value of α . On the other hand, it calls for the refinement of the distribution of Gaussians to fill areas lacking geometric features while splitting regions where Gaussians are overly large and overlapping. These regions tend to exhibit substantial position gradients. Therefore, based on the average position gradients within a certain number of iterations, we can identify the 3D Gaussians requiring adjustments through a threshold $t_{pos} = 0.0002$. For Gaussians that are too small to represent geometric details, we clone the Gaussians and move them a certain distance in the direction of the positional gradients. For those that are excessively large and overlapping, we split them and divide their scale by a hyperparameter $\xi = 1.6$.

It is clear that 3D Gaussians are only appropriate for representing static scenes. Changing its highly customized rendering pipeline directly not only contradicts the original intent of the differentiable rasterization pipeline of 3D Gaussians, but it is also difficult to modify. To enable 3D Gaussians to represent dynamic scenes while retaining the practical physical meaning of their individual learnable components, we decided to learn 3D Gaussians in canonical space and use an additional deformation field to learn the position and shape variations of the 3D Gaussians.

3.2. Deformable 3D Gaussians

An intuitive solution to model dynamic scene using 3D Gaussians is to separately train point cloud set in each time-dependent view collection and then perform interpolation between each set as a post-process, this can be practical for an MVS capture at a certain moment but not for a monocular capture in a temporal sequence. To handle the latter, a more general case in collection, we propose to jointly learn a deformation field along with 3D Gaussians.

We decouple the motion and geometry structure by leveraging a deformation network alongside with 3D Gaussians, converting the learning process into a canonical space to obtain time-independent 3D Gaussians. This decoupling approach introduces geometric priors of the scene, associating the changes in the positions of the 3D Gaussians with both time and coordinates, thereby distinguishing between static and dynamic parts. The deformation network is an MLP that takes as input time t and detached position x , and output offsets to transform the position and shape of 3D Gaussians in canonical space:

$$(\delta x, \delta r, \delta s) = \mathcal{F}_\theta(\gamma(x), \gamma(t)), \quad (4)$$

Method	Hell Warrior			Mutant			Hook			Bouncing Balls		
	PSNR↑	SSIM↑	LPIPS↓	PSNR↑	SSIM↑	LPIPS↓	PSNR↑	SSIM↑	LPIPS↓	PSNR↑	SSIM↑	LPIPS↓
3D-GS	29.89	0.9155	0.1056	24.53	0.9336	0.0580	21.71	0.8876	0.1034	23.20	0.9591	0.0600
D-NeRF	24.06	0.9440	0.0707	30.31	0.9672	0.0392	29.02	0.9595	0.0546	38.17	0.9891	0.0323
TiNeuVox	27.10	0.9638	0.0768	31.87	0.9607	0.0474	30.61	0.9599	0.0592	40.23	0.9926	0.0416
Tensor4D	31.26	0.9254	0.0735	29.11	0.9451	0.0601	28.63	0.9433	0.0636	24.47	0.9622	0.0437
K-Planes	24.58	0.9520	0.0824	32.50	0.9713	0.0362	28.12	0.9489	0.0662	40.05	0.9934	0.0322
Ours	41.03	0.9855	0.0251	42.29	0.9949	0.0052	36.86	0.9850	0.0162	40.82	0.9950	0.0095
Method	Lego			T-Rex			Stand Up			Jumping Jacks		
	PSNR↑	SSIM↑	LPIPS↓	PSNR↑	SSIM↑	LPIPS↓	PSNR↑	SSIM↑	LPIPS↓	PSNR↑	SSIM↑	LPIPS↓
3D-GS	22.10	0.9384	0.0607	21.93	0.9539	0.0487	21.91	0.9301	0.0785	20.64	0.9297	0.0828
D-NeRF	25.56	0.9363	0.0821	30.61	0.9671	0.0535	33.13	0.9781	0.0355	32.70	0.9779	0.0388
TiNeuVox	26.64	0.9258	0.0877	31.25	0.9666	0.0478	34.61	0.9797	0.0326	33.49	0.9771	0.0408
Tensor4D	23.24	0.9183	0.0721	23.86	0.9351	0.0544	30.56	0.9581	0.0363	24.20	0.9253	0.0667
K-Planes	28.91	0.9695	0.0331	30.43	0.9737	0.0343	33.10	0.9793	0.0310	31.11	0.9708	0.0468
Ours	33.07	0.9794	0.0183	37.16	0.9919	0.0107	43.41	0.9938	0.0077	36.86	0.9883	0.0143

Table 1. **Quantitative comparison on synthetic dataset.** We compare our method to several previous approaches: 3D-GS [15], D-NeRF [33], TiNeuVox [11], Tensor4D [37] and K-Planes [35] on full resolution test images. This may cause some methods to perform worse than the original paper because they downsample images by default. We color each cell as **best** and **second best**. It is worth noting that we observed a discrepancy in the scenarios presented in the training and test sets of the Lego in D-NeRF dataset. This can be substantiated by examining the flip angles of the Lego shovels. To ensure a meaningful comparison, we opted to utilize the validation set of Lego as the test set in our experiments.

where γ denotes the positional encoding:

$$\gamma(p) = (\sin(2^k \pi p), \cos(2^k \pi p))_{k=0}^{L-1}, \quad (5)$$

where $L = 10$ for x and $L = 6$ for t in synthetic scenes, while $L = 10$ for both x and t in real scenes. We set depth of deformation network $D = 8$ and the dimension of hidden layer $W = 256$. Experiments demonstrate that applying positional encoding to the inputs of the deformation network can enhance the details in rendering results.

3.3. Annealing Smooth Training

Many real datasets suffer from the issue of inaccurate pose estimation, especially for those dynamic scene collection. Training under imprecise poses can lead to overfitting on the training data. Moreover, as also mentioned in HyperNeRF [30], the imprecise poses from colmap for real datasets can cause spatial margin between each frame w.r.t. the test or train set, resulting in a noticeable deviation when rendering the test image compared to the ground truth. Previous methods employing implicit representations benefited from the inherent smoothness of the MLP, rendering the impact of such minor offsets on the final rendering results relatively inconspicuous. However, explicit point cloud rendering tends to amplify this effect. For monocular dynamic scenes, novel viewpoint rendering at a fixed time remains unaffected. However, for the task involving interpolated time, this kind of inconsistent scene in different time can lead to irregular rendering jitters.

To address this issue, we propose a novel adaptive smooth training mechanism specifically designed for

monocular dynamic scenes:

$$\begin{aligned} (\delta x, \delta r, \delta s) &= \mathcal{F}_\theta(\gamma(x), \gamma(t) + \mathcal{X}(i)), \\ \mathcal{X}(i) &= \mathcal{N}(0, 1) \cdot f_s \cdot (1 - \frac{i}{i_{thresh}}), \end{aligned} \quad (6)$$

where \mathcal{X} denotes the linearly decaying Gaussian noise. Here i is the current training iteration and we empirically set $f_s = 0.1$ and $i_{thresh} = 20k$.

Compared to the smooth loss introduced by methods of [33, 37], our approach does not incur additional computational overhead. It can enhance the model's temporal generalization in the early stages of training, as well as prevent excessive smoothing in the later stages, thus preserving the details of objects in dynamic scenes. Concurrently, it reduces the jitter observed in real datasets during time interpolation tasks.

4. Experiment

In this section, we present the experimental evaluation of our method. To give a proof of effectiveness, we evaluate our approach on the benchmark which consists of D-NeRF [33] synthetic dataset and HyperNeRF real dataset. The division on training and testing part, as well as the image resolution, aligns perfectly with the original paper.

Regarding the baselines, we primarily compare our method against the state-of-the-art (SOTA) approaches that are most closely related to our work. For synthetic datasets, we compared the following works: TiNeuVox [11], K-Planes [35], Tensor4D [37], D-NeRF [33] and original 3D Gaussians (3D-GS) [15]. For real monocular dataset, we



Figure 3. **Qualitative comparisons of baselines and our method on monocular synthetic dataset.** We visualize each scene using baselines and our method. Experimental results indicate that our approach recover more details when rendering novel viewpoints and can reconstruct delicate structure overtime, such as hand or skeleton.

compared HyperNeRF [30], TiNeuVox [11] and 3D-GS. Among these baselines, D-NeRF, HyperNeRF, and TiNeuVox represent dynamic scenes by transforming coordinates

into canonical space. In contrast, Tensor4D and K-Planes directly utilize discrete structures to learn a compact time-conditioned 4D feature. It should be noted that 3D-GS is a



Figure 4. **Ablation study.** We conduct ablation studies focusing on the annealing smooth training scheme within real datasets, wherein pe signifies the positional encoding over time. Compared with the reduced order (a) and the original order (b) of positional encoding over time, it becomes evident that the annealing smooth training strategy (c) effectively preserves high-frequency information. Simultaneously, it mitigates the temporal overfitting challenges instigated by imprecise pose estimations.

method designed for modeling static scenes. We visualize this method here to demonstrate that the improvements in our metrics are not solely reliant on the enhancements of the static regions by 3D-GS in the whole scene.

4.1. Implementation Details

We implement our deformation network with PyTorch [31] and keep the differential Gaussian rasterization presented by 3D-GS [15]. For training, we conducted training for a total of 40k iterations. During the initial 3k iterations, we solely trained the 3D Gaussians to attain relatively stable positions and shape, which would facilitate better convergence of the deformation field. Subsequently, we jointly train the 3D Gaussians and the deformation field. For optimization, a single Adam optimizer [16] is used but with different learning rate for each component: the learning rate of 3D gaussians is exactly the same as official implementation, while the learning rate of the deformation network undergoes exponential decay, ranging from 8e-4 to 1.6e-6. Adam’s β value range is set to (0.9, 0.999). All the experiments was done on one Tesla V100 with 32GB memory.

4.2. Results and Comparisons

Comparisons on synthetic dataset. We compare our method with the baselines on monocular synthetic dataset. Quantitative results are shown in Tab. 1. All metric strongly substantiate that our method surpasses existing state-of-the-art approaches, particularly in terms of structural consistency, where our LPIPS and SSIM exhibit more pronounced advantages. Qualitative results are shown in Fig. 3, which further affirm, from a visual perspective, that our method can achieve high-fidelity dynamic scene modeling, offering greater consistency and rendering detail in new viewpoint renderings.

Comparisons on real dataset. We compare our method with the baselines on monocular real dataset provided by HyperNeRF [30]. The qualitative results are presented in Fig. 5. This experimental result also shows that our method can be applied to real scenes, even if its pose is not completely accurate. We didn’t show the quantitative result because it’s meaningless due to an inaccurate pose on test set.

Depth Visualization. We visualized the depth of various synthetic dataset scenes in Fig. 6 to demonstrate that our deformation network is well fitted to produce transforming information at each time rather than being hard-coded based on color. The precise depth underscores the accuracy of our geometric reconstruction, which also elucidates our exemplary performance on the LPIPS/SSIM metrics, proving highly advantageous for the task of new viewpoint synthesis.

4.3. Ablation Study

Annealing smooth training mechanism. Fig. 4 demonstrates that this mechanism aids the framework in converging to more detailed regions, reducing the overfitting phenomenon observed in real datasets. It is evident that this training mechanism can enhance the temporal smoothness of the deformation field.

5. Limitations

Through our experimental evaluations, we observed that the convergence of 3D Gaussians is profoundly influenced by the diversity of perspectives. As a result, datasets characterized by sparse viewpoints and limited viewpoint coverage may lead our method to encounter overfitting challenges. Additionally, the efficacy of our approach is contingent upon the accuracy of pose estimations. This dependency was evident when our method did not achieve op-

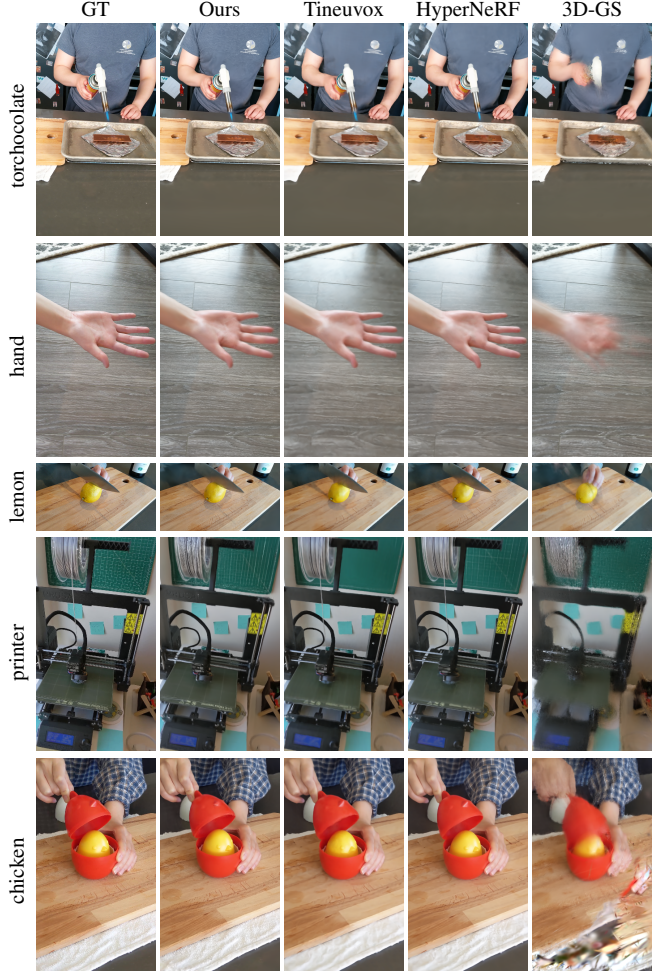


Figure 5. Qualitative comparisons of baselines and our method on monocular real dataset. The first three rows present the results of the time interpolation task, while the last two rows depict the outcomes of the novel viewpoint synthesis task. Experimental results indicate that our method can achieve superior rendering quality on real datasets where the pose is not absolutely precise. Notably, metrics designed to assess image rendering quality, such as PSNR, tend to impose greater penalties on minor offsets. Consequently, our method’s quantitative metrics may not consistently surpass those of methods that produce overly blurred results under conditions of imprecise camera poses, even though our rendered images tend to exhibit reduced artifacts and present greater clarity. A similar observation has been documented in HyperNeRF [30].

timal PSNR values on the Nerfies/HyperNeRF dataset, attributable to deviations in pose estimation via COLMAP. Furthermore, the temporal complexity of our approach is directly proportional to the quantity of point clouds. In scenarios with an extensive array of point clouds, there is a potential escalation in both training duration and memory consumption. It is also noteworthy that our current evaluations have been restricted to data with non-intense motion

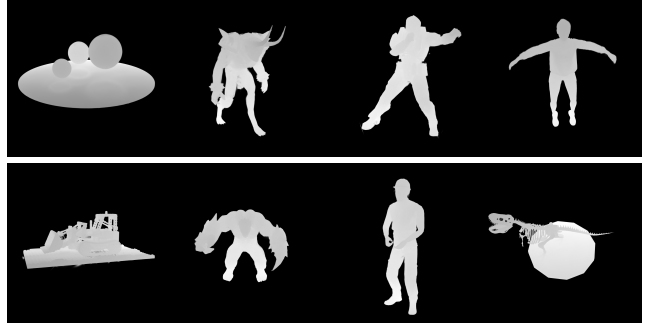


Figure 6. Depth Visualization. We visualized the depth of the D-NeRF dataset. The first row includes bouncing-balls, hell-warrior, hook, and jumping jacks, while the second row includes lego, mutant, standup, and trex.

variations. The applicability of our method to intricate human movements, such as facial alterations, remains an uncharted domain. We perceive these constraints as promising directions for subsequent research endeavors.

6. Conclusions

We proposed a deformable 3D Gaussian splatting approach for dynamic scene modeling that achieves higher quality than previously. We increased the applicability of the 3D-GS differentiable rendering pipeline in monocular dynamic scenes by learning the 3D Gaussians in canonical space. Point cloud-based solutions are more editable and post-production friendly than implicit representations. Furthermore, we introduced a linear decay smoothing mechanism to prevent over-fitting over time embedding. Unlike traditional smooth loss, our mechanism incurs no additional training overhead while retaining more details. Experiment results show that our method achieves the best rendering effects in scenes with a large number of training viewpoints and is capable of real-time rendering.

References

- [1] Benjamin Attal, Eliot Laidlaw, Aaron Gokaslan, Changil Kim, Christian Richardt, James Tompkin, and Matthew O’Toole. Törf: Time-of-flight radiance fields for dynamic scene view synthesis. *Advances in Neural Information Processing Systems*, 34:26289–26301, 2021. [3](#)
- [2] Jonathan T. Barron, Ben Mildenhall, Matthew Tancik, Peter Hedman, Ricardo Martin-Brualla, and Pratul P. Srinivasan. Mip-nerf: A multiscale representation for anti-aliasing neural radiance fields. *ICCV*, 2021. [2, 3](#)
- [3] Jonathan T. Barron, Ben Mildenhall, Dor Verbin, Pratul P. Srinivasan, and Peter Hedman. Mip-nerf 360: Unbounded anti-aliased neural radiance fields. *CVPR*, 2022. [3](#)
- [4] Jonathan T. Barron, Ben Mildenhall, Dor Verbin, Pratul P. Srinivasan, and Peter Hedman. Zip-nerf: Anti-aliased grid-based neural radiance fields. *ICCV*, 2023. [2, 3](#)

[5] Mark Boss, Raphael Braun, Varun Jampani, Jonathan T. Barron, Ce Liu, and Hendrik P.A. Lensch. Nerd: Neural reflectance decomposition from image collections. In *IEEE International Conference on Computer Vision (ICCV)*, 2021. 2

[6] Ang Cao and Justin Johnson. Hexplane: A fast representation for dynamic scenes. *CVPR*, 2023. 3

[7] Anpei Chen, Zexiang Xu, Andreas Geiger, Jingyi Yu, and Hao Su. Tensorf: Tensorial radiance fields. In *European Conference on Computer Vision (ECCV)*, 2022. 2, 3

[8] Zhiqin Chen, Thomas Funkhouser, Peter Hedman, and Andrea Tagliasacchi. Mobilenerf: Exploiting the polygon rasterization pipeline for efficient neural field rendering on mobile architectures. In *Proceedings of the IEEE/CVF Conference on Computer Vision and Pattern Recognition*, pages 16569–16578, 2023. 3

[9] Alvaro Collet, Ming Chuang, Pat Sweeney, Don Gillett, Dennis Evseev, David Calabrese, Hugues Hoppe, Adam Kirk, and Steve Sullivan. High-quality streamable free-viewpoint video. *ACM Transactions on Graphics (ToG)*, 34(4):1–13, 2015. 1

[10] Kangle Deng, Andrew Liu, Jun-Yan Zhu, and Deva Ramanan. Depth-supervised NeRF: Fewer views and faster training for free. In *Proceedings of the IEEE/CVF Conference on Computer Vision and Pattern Recognition (CVPR)*, June 2022. 2

[11] Jiemin Fang, Taoran Yi, Xinggang Wang, Lingxi Xie, Xiaopeng Zhang, Wenyu Liu, Matthias Nießner, and Qi Tian. Fast dynamic radiance fields with time-aware neural voxels. In *SIGGRAPH Asia 2022 Conference Papers*, 2022. 2, 3, 5, 6

[12] Stephan J Garbin, Marek Kowalski, Matthew Johnson, Jamie Shotton, and Julien Valentin. Fastnerf: High-fidelity neural rendering at 200fps. In *Proceedings of the IEEE/CVF International Conference on Computer Vision*, pages 14346–14355, 2021. 3

[13] Peter Hedman, Pratul P Srinivasan, Ben Mildenhall, Jonathan T Barron, and Paul Debevec. Baking neural radiance fields for real-time view synthesis. In *Proceedings of the IEEE/CVF International Conference on Computer Vision*, pages 5875–5884, 2021. 3

[14] Takeo Kanade, Peter Rander, and PJ Narayanan. Virtualized reality: Constructing virtual worlds from real scenes. *IEEE Multimedia*, 4(1):34–47, 1997. 1

[15] Bernhard Kerbl, Georgios Kopanas, Thomas Leimkühler, and George Drettakis. 3d gaussian splatting for real-time radiance field rendering. *ACM Transactions on Graphics*, 42(4), July 2023. 2, 3, 4, 5, 7

[16] Diederik Kingma and Jimmy Ba. Adam: A method for stochastic optimization. In *International Conference on Learning Representations (ICLR)*, 2015. 7

[17] Hao Li, Linjie Luo, Daniel Vlasic, Pieter Peers, Jovan Popović, Mark Pauly, and Szymon Rusinkiewicz. Temporally coherent completion of dynamic shapes. *ACM Transactions on Graphics (TOG)*, 31(1):1–11, 2012. 1

[18] Tianye Li, Mira Slavcheva, Michael Zollhoefer, Simon Green, Christoph Lassner, Changil Kim, Tanner Schmidt, Steven Lovegrove, Michael Goesele, Richard Newcombe, et al. Neural 3d video synthesis from multi-view video. In *Proceedings of the IEEE/CVF Conference on Computer Vision and Pattern Recognition*, pages 5521–5531, 2022. 3

[19] Zhaoshuo Li, Thomas Müller, Alex Evans, Russell H Taylor, Mathias Unberath, Ming-Yu Liu, and Chen-Hsuan Lin. Neuralangelo: High-fidelity neural surface reconstruction. In *IEEE Conference on Computer Vision and Pattern Recognition (CVPR)*, 2023. 2

[20] Chen-Hsuan Lin, Wei-Chiu Ma, Antonio Torralba, and Simon Lucey. Barf: Bundle-adjusting neural radiance fields. In *IEEE International Conference on Computer Vision (ICCV)*, 2021. 2

[21] Haotong Lin, Sida Peng, Zhen Xu, Yunzhi Yan, Qing Shuai, Hujun Bao, and Xiaowei Zhou. Efficient neural radiance fields for interactive free-viewpoint video. In *SIGGRAPH Asia Conference Proceedings*, 2022. 3

[22] Jia-Wei Liu, Yan-Pei Cao, Weijia Mao, Wenqiao Zhang, David Junhao Zhang, Jussi Keppo, Ying Shan, Xiaohu Qie, and Mike Zheng Shou. Devrf: Fast deformable voxel radiance fields for dynamic scenes. *Advances in Neural Information Processing Systems*, 35:36762–36775, 2022. 2

[23] Lingjie Liu, Jiatao Gu, Kyaw Zaw Lin, Tat-Seng Chua, and Christian Theobalt. Neural sparse voxel fields. *Advances in Neural Information Processing Systems*, 33:15651–15663, 2020. 3

[24] Yuan Liu, Peng Wang, Cheng Lin, Xiaoxiao Long, Jiepeng Wang, Lingjie Liu, Taku Komura, and Wenping Wang. Nero: Neural geometry and brdf reconstruction of reflective objects from multiview images. In *SIGGRAPH*, 2023. 2

[25] Jonathon Luiten, Georgios Kopanas, Bastian Leibe, and Deva Ramanan. Dynamic 3d gaussians: Tracking by persistent dynamic view synthesis. *preprint*, 2023. 2

[26] Julien N. P. Martel, David B. Lindell, Connor Z. Lin, Eric R. Chan, Marco Monteiro, and Gordon Wetzstein. Acorn: Adaptive coordinate networks for neural scene representation. *ACM Transactions on Graphics (SIGGRAPH)*, 40(4), 2021. 3

[27] Ben Mildenhall, Pratul P Srinivasan, Matthew Tancik, Jonathan T Barron, Ravi Ramamoorthi, and Ren Ng. Nerf: Representing scenes as neural radiance fields for view synthesis. *Communications of the ACM*, 65(1):99–106, 2021. 1, 2

[28] Thomas Müller, Alex Evans, Christoph Schied, and Alexander Keller. Instant neural graphics primitives with a multiresolution hash encoding. *ACM Transactions on Graphics*, 41(4):102:1–102:15, July 2022. 2

[29] Keunhong Park, Utkarsh Sinha, Jonathan T Barron, Sofien Bouaziz, Dan B Goldman, Steven M Seitz, and Ricardo Martin-Brualla. Nerfies: Deformable neural radiance fields. In *Proceedings of the IEEE/CVF International Conference on Computer Vision*, pages 5865–5874, 2021. 2

[30] Keunhong Park, Utkarsh Sinha, Peter Hedman, Jonathan T. Barron, Sofien Bouaziz, Dan B Goldman, Ricardo Martin-Brualla, and Steven M. Seitz. Hypernerf: A higher-dimensional representation for topologically varying neural radiance fields. *ACM Transactions on Graphics*, 40(6), dec 2021. 1, 2, 5, 6, 7, 8

[31] Adam Paszke, Sam Gross, Francisco Massa, Adam Lerer, James Bradbury, Gregory Chanan, Trevor Killeen, Zeming Lin, Natalia Gimelshein, Luca Antiga, et al. Pytorch: An imperative style, high-performance deep learning library. *Advances in Neural Information Processing Systems*, 32, 2019. [7](#)

[32] Sida Peng, Yunzhi Yan, Qing Shuai, Hujun Bao, and Xiaowei Zhou. Representing volumetric videos as dynamic mlp maps. In *CVPR*, 2023. [3](#)

[33] Albert Pumarola, Enric Corona, Gerard Pons-Moll, and Francesc Moreno-Noguer. D-nerf: Neural radiance fields for dynamic scenes. In *Proceedings of the IEEE/CVF Conference on Computer Vision and Pattern Recognition*, pages 10318–10327, 2021. [2, 5](#)

[34] Christian Reiser, Songyou Peng, Yiyi Liao, and Andreas Geiger. Kilonerf: Speeding up neural radiance fields with thousands of tiny mlps. In *Proceedings of the IEEE/CVF International Conference on Computer Vision*, pages 14335–14345, 2021. [3](#)

[35] Sara Fridovich-Keil and Giacomo Meanti, Frederik Rahbæk Warburg, Benjamin Recht, and Angjoo Kanazawa. K-planes: Explicit radiance fields in space, time, and appearance. In *CVPR*, 2023. [2, 3, 5](#)

[36] Johannes L Schonberger and Jan-Michael Frahm. Structure-from-motion revisited. In *Proceedings of the IEEE Conference on Computer Vision and Pattern recognition*, pages 4104–4113, 2016. [2, 3](#)

[37] Ruizhi Shao, Zerong Zheng, Hanzhang Tu, Boning Liu, Hongwen Zhang, and Yebin Liu. Tensor4d: Efficient neural 4d decomposition for high-fidelity dynamic reconstruction and rendering. In *Proceedings of the IEEE Conference on Computer Vision and Pattern Recognition*, 2023. [2, 3, 5](#)

[38] Liangchen Song, Anpei Chen, Zhong Li, Zhang Chen, Lele Chen, Junsong Yuan, Yi Xu, and Andreas Geiger. Nerf-player: A streamable dynamic scene representation with decomposed neural radiance fields. *IEEE Transactions on Visualization and Computer Graphics*, 29(5):2732–2742, 2023. [2, 3](#)

[39] Jonathan Starck and Adrian Hilton. Surface capture for performance-based animation. *IEEE Computer Graphics and Applications*, 27(3):21–31, 2007. [1](#)

[40] Cheng Sun, Min Sun, and Hwann-Tzong Chen. Direct voxel grid optimization: Super-fast convergence for radiance fields reconstruction. In *Proceedings of the IEEE/CVF Conference on Computer Vision and Pattern Recognition*, pages 5459–5469, 2022. [3](#)

[41] Edgar Tretschk, Ayush Tewari, Vladislav Golyanik, Michael Zollhöfer, Christoph Lassner, and Christian Theobalt. Non-rigid neural radiance fields: Reconstruction and novel view synthesis of a dynamic scene from monocular video. In *Proceedings of the IEEE/CVF International Conference on Computer Vision*, pages 12959–12970, 2021. [3](#)

[42] Chaoyang Wang, Ben Eckart, Simon Lucey, and Orazio Gallo. Neural trajectory fields for dynamic novel view synthesis. *arXiv preprint arXiv:2105.05994*, 2021. [2](#)

[43] Liao Wang, Jiakai Zhang, Xinhang Liu, Fuqiang Zhao, Yan-shun Zhang, Yingliang Zhang, Minye Wu, Jingyi Yu, and Lan Xu. Fourier plenoctrees for dynamic radiance field rendering in real-time. In *Proceedings of the IEEE/CVF Conference on Computer Vision and Pattern Recognition (CVPR)*, pages 13524–13534, June 2022. [2](#)

[44] Peng Wang, Lingjie Liu, Yuan Liu, Christian Theobalt, Taku Komura, and Wenping Wang. Neus: Learning neural implicit surfaces by volume rendering for multi-view reconstruction. *NeurIPS*, 2021. [2](#)

[45] Peng Wang, Yuan Liu, Zhaoxi Chen, Lingjie Liu, Ziwei Liu, Taku Komura, Christian Theobalt, and Wenping Wang. F2-nerf: Fast neural radiance field training with free camera trajectories. *CVPR*, 2023. [2, 3](#)

[46] Peng Wang, Lingzhe Zhao, Ruijie Ma, and Peidong Liu. BAD-NeRF: Bundle Adjusted Deblur Neural Radiance Fields. In *Proceedings of the IEEE/CVF Conference on Computer Vision and Pattern Recognition (CVPR)*, pages 4170–4179, June 2023. [2](#)

[47] Zirui Wang, Shangzhe Wu, Weidi Xie, Min Chen, and Victor Adrian Prisacariu. NeRF—: Neural radiance fields without known camera parameters. *arXiv preprint arXiv:2102.07064*, 2021. [2](#)

[48] Wenqi Xian, Jia-Bin Huang, Johannes Kopf, and Changil Kim. Space-time neural irradiance fields for free-viewpoint video. In *Proceedings of the IEEE/CVF Conference on Computer Vision and Pattern Recognition*, pages 9421–9431, 2021. [2](#)

[49] Jiawei Yang, Marco Pavone, and Yue Wang. Freenerf: Improving few-shot neural rendering with free frequency regularization. In *Proc. IEEE Conference on Computer Vision and Pattern Recognition (CVPR)*, 2023. [2](#)

[50] Alex Yu, Rui long Li, Matthew Tancik, Hao Li, Ren Ng, and Angjoo Kanazawa. PlenOctrees for real-time rendering of neural radiance fields. In *ICCV*, 2021. [2, 3](#)

[51] Xiuming Zhang, Pratul P Srinivasan, Boyang Deng, Paul Debevec, William T Freeman, and Jonathan T Barron. Nerfactor: Neural factorization of shape and reflectance under an unknown illumination. *ACM Transactions on Graphics (ToG)*, 40(6):1–18, 2021. [2](#)

[52] Matthias Zwicker, Hanspeter Pfister, Jeroen Van Baar, and Markus Gross. Ewa volume splatting. In *Proceedings Visualization, 2001. VIS'01.*, pages 29–538. IEEE, 2001. [4](#)